We are IntechOpen, the world's leading publisher of Open Access books Built by scientists, for scientists

4,800
Open access books available

122,000
International authors and editors

135M
Downloads

Our authors are among the

154
Countries delivered to

TOP 1%
most cited scientists

12.2%
Contributors from top 500 universities

CLARIVATE ANALYTICS BOOK CITATION INDEX INDEXED

WEB OF SCIENCE™

Selection of our books indexed in the Book Citation Index in Web of Science™ Core Collection (BKCI)

Interested in publishing with us?
Contact book.department@intechopen.com

Numbers displayed above are based on latest data collected.
For more information visit www.intechopen.com

15

Magnetohydrodynamics of Metallic Foil Electrical Explosion and Magnetically Driven Quasi-Isentropic Compression

Guiji Wang, Jianheng Zhao, Binqiang Luo and Jihao Jiang
Institute of Fluid Physics, China Academy of Engineering Physics, Mianyang City, Sichuan Province China

1. Introduction

The electrical explosion of conductors, such as metallic foils and wires, refers to rapid changes of physical states when the large pulsed current (tens or hundreds of kA or more, the current density $j \geq 10^6$ A/cm^2) flows through the conductors in very short time(sub microsecond or several microseconds), which may produce and radiate shock waves, electrical magnetic waves, heat and so on. There are many applications using some characteristics of the electrical explosion of conductors.

The Techniques of metallic foil electrical explosion had been developed since 1961, which was first put forward by Keller, Penning[1] and Guenther et al[2]. However, it develops continually until now because of its wide uses in material science, such as preparation of nanometer materials and plating of materials[3,4], shock wave physics[5-7] , high energy density physics[8] and so on. Especially the techniques of metallic foil electrically exploding driving highvelocity flyers, are widely used to research the dynamics of materials, hypervelocity impact phenomena and initiation of explosives in weapon safety and reliability. Therefore, in this chapter we focus on the physical process of metallic foil explosion and the techniques of metallic foil electrically exploding driving highvelocity flyers. Here the explosion of metallic foils are caused by the large current flowing through in sub microsecond or 1～2 microsecond or less. During the whole physical process, not only does the temperature rising, melting, vaporizing and plasma forming caused by instantaneously large current, but also the electrical magnetic force exists and acts on. Because the whole process is confined by rigid face and barrel, and the time is very short of microsecond or sub microsecond or less, and the phynomena is similar to the explosion of explosives, we call the process electrical explosion of metallic foils. This process is a typically hydrodynamic phenomena. It is also a magnetohydrodynamic process because of the exist and action of the magnetic force caused by large current and self-induction magnetic field.

Magnetically driven quasi-isentropic compression is an relatively new topic, which was developed in 1972[9]. At that time the technique of magnetically driven quasi-isentropic compression was used to produce high pressure and compress the cylindrical sample materials. Until 2000, the planar loading technique of magnetically driven quasi-isentropic

compression was firstly presented by J.R. Asay at Sandia National Laboratory[10]. In last decade, this planar loading technique had being developed fastly and accepted by many researchers in the world, such as France[11], United Kingdom[12],and China[13]. As J.R. Asay said, it will be a new experimental technique widely used in shock dynamics, astrophysics, high energy density physics, material science and so on. The process of magnetically driven quasi-isentropic compression is typical magnetodynamics[14], which refers to dynamic compression, magnetic field diffusion, heat conduction and so on.

As described above, the electrical explosion of metallic foil and magnetically driven quasi-isentropic compression is typically magnetohydrodynamic problem. Although it develops fastly and maybe many difficulties and problems exist in our work, we present our important and summary understanding and results to everyone in experiments and simulations of electrical explosion of metallic foil and magnetically driven quasi-isentropic compression in last decade.

In the following discussions, more attentions are paid to the physical process, the experimental techniques and simulation of electrical explosion of metallic foil and magnetically driven quasi-isentropic compression.

2. Physical process of metallic foil electrical explosion and magnetically driven quasi-isentropic compression

2.1 Metallic foil electrical explosion

Here we introduce the model of metallic foil electrically exploding driving highvelocity flyers to describe the physical process of electrical explosion of metallic foil shown in Fig.1. A large pulsed current is released to the metallic foil of the circuit, which is produced by a typically pulsed power generator. The circuit can be described by *R-C-L* electrical circuit equations[15]. During the circuit, the metallic foil is with larger resistance than that of other part, so the energy is mainly absorbed by the metallic foil, and then the physical states of metallic foil change with time. Fig.2 shows the typical current and voltage histories between metallic aluminum foil during the discharging process of pulsed power generator.

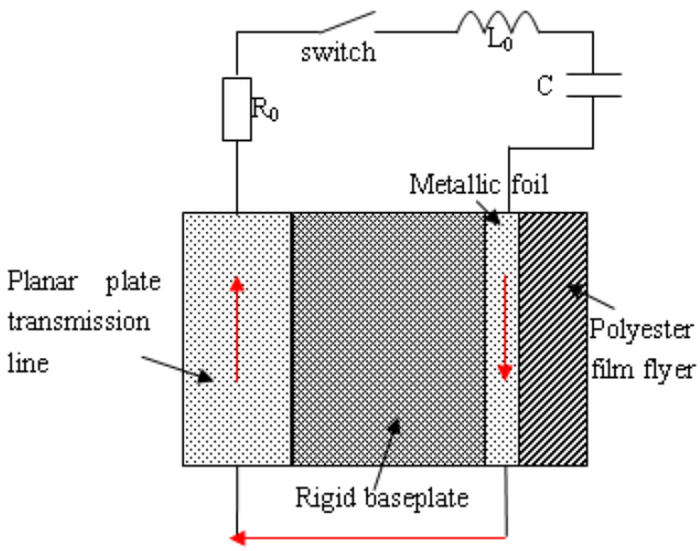

Fig. 1. The model of metallic foil electrically exploding driving highvelocity flyers.

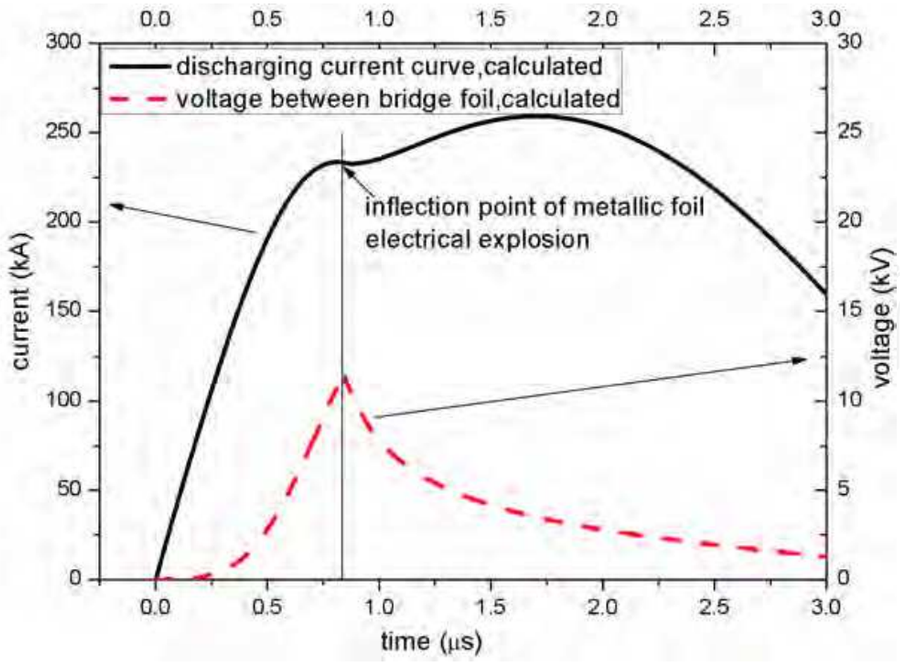

Fig. 2. The typically discharging current and voltage histories between bridge Aluminum foil.

According to the density changing extent of metallic foil when the first pulsed current flows through it, the whole process of electrical explosion of metallic foil can be classified to two stages. The initial stage includes the heating stage , the melting stage and the heating stage of liquid metal before vaporizing. During this process, the density of metallic foil changes relatively slow. The second stage includes the vaporizing stage and the following plasma forming. The typical feature of electrical explosion of metallic foil is that the foil expands rapidly and violently, and that the resistance increases to be two or more orders than that of initial time ($R/R_0 \sim 100$). The resistance increases to be maximum when the state of metallic foil is at the vaporizing stage. During this stage, the voltage of between foil also increases to be maximum, and then the breakdown occurs and the plamas is forming. The inflection point of the discharging current shown in Fig.2 exhibits the feature.

At the initial satge, the expansion of metallic foil is not obvious, and the change of physical states can be described with one thermodynamic variable T (temperature) or specific enthalpy. The energy loss of the interaction between the foil and the ambient medium can be neglected when there is no surface voltaic arcs. Therefore, some assumptions can be used to simplify the problem. We can think that the heating of the metallic foil is uniform and the instability, heat conduction and skin effect can not be considered at initial stage. For this stage, the physical states of metallic foil vary from solid to liquid, and the model of melting phase transition can be used to described it well[16].

For the second stage, the physical states varies from liquid to gas, and then from gas to plasma. There are several vaporizing mechanisms to describe this transition, such as surface evaporation and whole boil[16]. The rapid vaporizing of liquid metal make its resistance increases violently, and the current decreases correspondingly. At this time, the induction voltage between bridge foil increases fastly. If the induction voltage can make the metallic vapor breakdown and the plasma is formed, the circuit is conducted again. Of course, the

breakdown of metallic vapor needs some time, which is called relaxation time as shown in Fig.3. For different charging voltages, the relaxation time varies, which can be seen from the experimental current hostories in Fig.3.

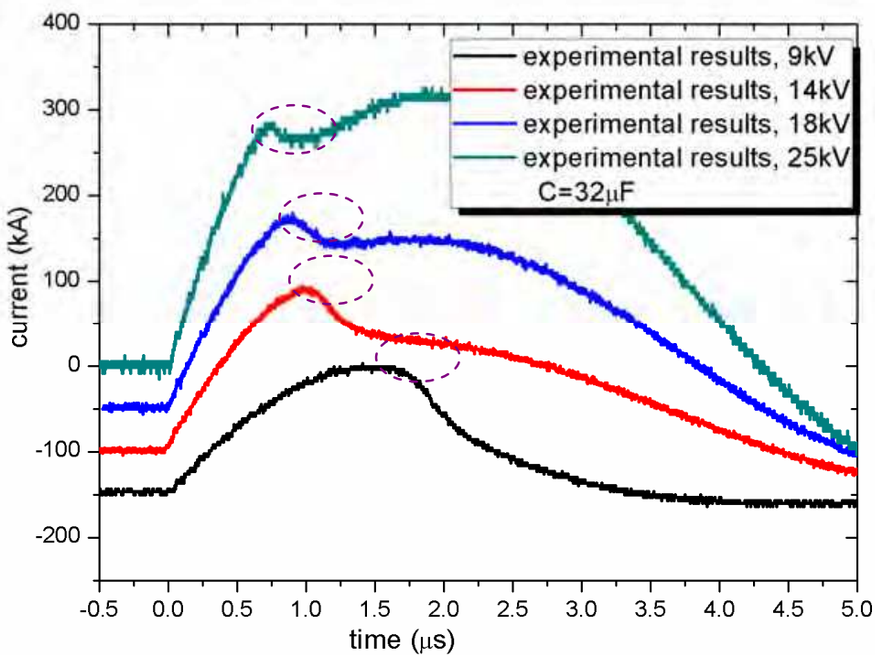

Fig. 3. The breakdown relaxation time shown in the discharging current histories at different charging voltage for the pulsed power generator.

One important application of the electrical explosion of metallic foil is to launch highvelocity flyers with the rapid expansion of tha gas and plasma from electrical explosion of metallic foil. Some metallic materials are with good conductivity and explosion property, such as gold, silver, copper, aluminum and so on. The experimental results[17] show that the aluminum foil is the best material for the application of metallic foil electrically exploding driven highvelocity flyers. There are many models used to describe the process, such as eletrical Gurney model[18], Schmidt model[19] and one dimensional magnetohydrodynamic model[20]. The electrical Gurney model and Schmidt model are two empirical models which are derived from energy conservation equation based on some assumptions. For a specific electrical parameters of the circuit of some apparatus, the electrical Gurney model can be used to predict the final velocity of the flyers when the Gurney parameters are determined based on some experimental results. And the Schmidt model can be used to predict the velocity history of the flyers because the Gurney energy part is substituted with an energy part with the function of time, which is depended on the measured current and voltage histories between bridge foil to correct the specific power coefficient. These two models can't reflect other physical variables of electrical explosion of metallic foil except the velocity of the flyer. Therefore, a more complex model is put forward based on magnetohydrodynamics, which considers heat conduction, magnetic pressure and electrical power. The magnetohydrodynamic model can well reflect the physical process of electrical explosion of metallic foil. The equations are given below[16,20].

$$\begin{cases} \dot{x} = u; \ \dot{\mathrm{v}} = \dfrac{\partial}{\partial q}(x^{\gamma-1}u) \\ \dot{u} + x^{\gamma-1}\dfrac{\partial}{\partial q}(p + p_{\omega} + \dfrac{B^2}{2\mu_0}) = 0 \\ \dot{\epsilon} + (p + p_{\omega})\dot{\mathrm{v}} = Q_{\mathrm{v}} \\ \dfrac{d}{dt}(x^{1-\gamma}\,\mathrm{v}\,B) = \dfrac{\partial E}{\partial q} \\ E = \dfrac{1}{\mu_0\sigma\,\mathrm{v}}\dfrac{\partial}{\partial q}(x^{\gamma-1}B) \\ j = \sigma E; \ Q_{\mathrm{v}} = \mathrm{v}\,jE \\ p = p(\mathrm{v},T); \ \epsilon = \epsilon(\mathrm{v},T); \quad \sigma = \sigma(\mathrm{v},T) \end{cases} \tag{1}$$

Where, γ—symmetric exponent（for metallic wire or cylindrical foil γ=2，and for planar foil γ=1）; ∂/∂q=x$^{1-\gamma}$v∂/∂x; q—Lagrange mass coordinate;B—transverse component of magnetic field;E—axial component of electrical field; j—current density; Q_{V}—specific power of Joule heating; p_{ω}—artificial viscosity coefficient；u—transverse moving velocity；p—pressure;ϵ—internal energy; v—unit volume; σ—conductivity.

For this apparatus, the discharging ciruit is a typical *RCL* circuit, which can be expressed by equation（2）below.

$$\begin{cases} \dfrac{d}{dt}\left[(L_0 + L_{foil})I\right] + U_{foil} + R_0 I = U_c; \\ \dfrac{dU_C}{dt} = -\dfrac{I}{C_0}; \\ U_{foil} \simeq l_{foil}E\left[t, X(t)\right] \ , \end{cases} \tag{2}$$

In the equation (2), when the time t=0, the primary current and voltage I（0）=0 and $U_{\mathrm{c}}(0)$= U_0, C_0 and U_0 are the capacitance and charging voltage of capacitor or capacitor bank, L_0 and R_0 are the inductance and efficient resistance of circuit, U_{foil} is the voltage between the ends of metallic foil, which is related with the length l_{foil} of metallic foil and the magetic field of the space around the foil. the dynamic inductance L_{foil} can be obtained by equation (3).

$$L_{foil}(t) = \mu_0 k(l_{foil} / b)\left[x_0^{'} - X_0\right] \tag{3}$$

Where μ_0 is the vacuum magnetic permeability, k is a coefficient related with the length l and width b of metallic foil. x is the expanding displacement of metallic foil.

2.2 Magnetically driven quasi-isentropic compression

The concept of magnetically driven quasi-isentropic compression is illustrated in Fig.4. A direct short between the anode and cathode produces a planar magnetic field between the conductors when a pulsed current flows through the electrodes over a time scale of 300～800ns. The interaction between the current (density J) and the induction magnetic field

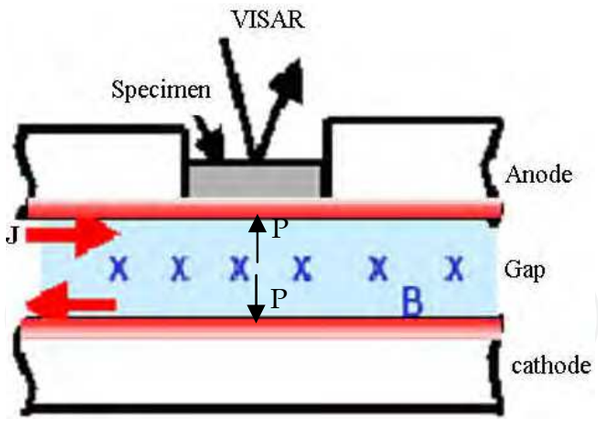

Fig. 4. The principle diagram of magnetically driven quasi-isentropic compression.

B produces the magnetic pressure ($\vec{J} \times \vec{B}$) proportional to the square of the field. The force is loaded to the internal surface that the current flows through. The loading pressure wave is a ramp wave, which is a continuous wave. Compared with the shock wave, the increment of temperature and entropy is very lower. However, because of the effects of viscosity and plastic work, the sample can't turn back to the original state after the loading wave. That is to say, in solids the longitudinal stress differs from the hydrostatic pressure because of resolved shear stresses that produce an entropy increase from the irreversible work done by deviator[21, 22]. For this reason, the ramp wave loading process is usually assumed to be quasi-isentropic compression. Besides the loading force is magnetic pressure, it is called magnetically driven quasi-isentropic compression.

In order to produce high pressure, the amplitude of the current is ususally up to several megamperes or tens of megamperes. Because of the effects of Joule heating and magnetic field diffusion, the physical states of the loading surface will change from solid to liquid, and to gas and plasma. And these changes will propagate along the thickness direction of the electrodes originated from the loading surface. These phenomena are typically magnetohydrodynamic problems. In order to describe the physical process, the equation of magnetic field diffusion is considered besides the equations of mass, momentum and energy. The magnetohydrodynamic equations are presented below.

$$\begin{cases} \dfrac{\partial \rho_m}{\partial t} + \nabla \cdot \left(\rho_m \vec{u} \right) = 0 \\ \rho_m \dfrac{d\vec{u}}{dt} + \nabla \left(p + q \right) - \vec{J} \times \vec{B} = 0 \\ \dfrac{de}{dt} + \left(p + q \right) \dfrac{d(1/\rho_m)}{dt} - \dot{e}_D = 0 \\ \rho_m \dfrac{d}{dt} \left(\dfrac{\vec{B}}{\rho_m} \right) - \left(\vec{B} \cdot \nabla \right) \vec{u} = -\nabla \times \left[\dfrac{\eta}{\mu_0} \left(\nabla \times \vec{B} \right) \right] \\ \vec{J} = \sigma \vec{E} = \dfrac{1}{\mu_0} \nabla \times \vec{B} \\ \vec{u} = \dfrac{d\vec{x}}{dt}, \dot{e}_D = \kappa \nabla T \end{cases} \tag{4}$$

Where ρ_m is mass density of electrodes, u is velocity, J is current density, B is magnetic field, p is pressure, q is artificial viscosity pressure, e is specific internal energy, σ is electrical conductivity of electrodes and κ is thermal conducitivity.

Similar to the technique of electrical explosion of metallic foil, the large current is also produced by some pulsed power generators, for example, the ZR facility at Sandia National Laboratory can produce a pulsed current with peak value from 16 MA to 26 MA and rising time from 600 ns to 100 ns[23]. In the following part, we will introduce the techniques of magnetically driven quasi-isentropic compression based on the pulsed power generators developed by ourselves.

3. Techniques of metallic foil electrically exploding driving highvelocity flyers and magnetically driven quasi-isentropic compression

The techniques of metallic foil electrically exploding driving highvelocity flyers and magnetically driven quasi-isentropic compression have been widely used to research the dynamic properties of materials and highvelocity impact phenomena in the conditions of shock and shockless(quasi-isentropic or ramp wave) loading. By means of these two techniques, we can know the physical, mechnical and thermodynamic properties of materials over different state area (phase space), such as Hugoniot and off-Hugoniot states.

3.1 Metallic foil electrically exploding driving highvelocity flyers[24,25,26]

As descibed above, the high pressure gas and plasma are used to launch highvelovity flyer plates, which are produced from the electrical explosion of metallic foil. The working principle diagram of the metallic foil electrically exploding driving highvelocity flyers is presented in Fig.5. Usually we choose the pure aluminum foil as the explosion material because of its good electrical conductivity and explosion property. The flyers may be polyester films, such as Mylar or Kapton, or complex ones consisted of polyester film and metallic foil. The material of barrel for accelerating the flyers may be metals or non-polyester films, such as Mylar or Kapton, or complex ones consisted of polyester film and metallic foil. The material of barrel for accelerating the flyers may be metals or non-metals, such as

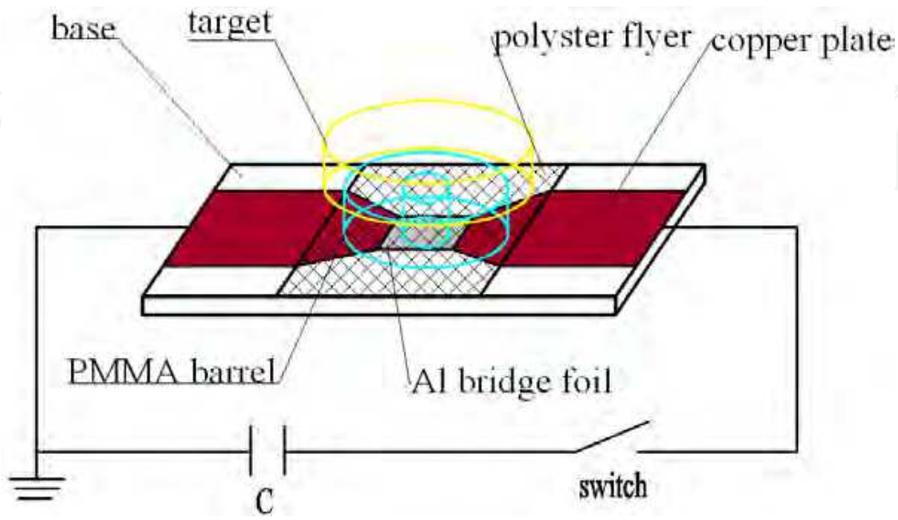

Fig. 5. The diagram of working principle of metallic foil electrically exploding driving flyer.

ceramics, steel or acryl glass. The base plate is used to confined the high pressure gas and plasma and reflect them to opposite direction to propel the flyers. The base plate also insulates the anode from the cathode transimission lines. So the material of base plate is non-metal and the ceramics is a good one.

The whole working process is that the large current flows through the metallic foil instantly and the metallic foil goes through from solid, to liquid, gas and plasma, and then the high pressure gases and plasmas expand to some direction to drive the polyester Mylar flyer to high velocity and impacts the targets.

Based on low inductance technologies of pulsed storaged energy capacitor, detonator switch and parallel plate transmission lines with solid films insulation, two sets of experimental apparatuses with storaged energy of 14.4 kJ and 40 kJ were developed for launching hypervelocity flyer. The first apparatus is only consisted of one storaged energy pulsed capcitor with capacitance of 32 μF, inductance of 30 nH and rated voltage of 30 kV. The parallel plate transmission lines and solid insulation films are used, which are with very low inducatnce. The thickness of insulation films is no more than 1 mm, which is composed of several or ten pieces of Mylar films with thichness of 0.1 mm. The second apparatus is composed of two capacitors with capacitance of 16 μF and rated voltage of 50 kV in parallel. For two apparatuses, the detonator switch is used, which is with low inductance of about 7 nH and easy to connected with the parallel plate transmission lines.

Fig.6 shows the diagram of the detonator switch. The detonator is exploded and the explosion products make the aluminum ring form metallic jet and breakdown the insulation films between anode and negative electrodes, and then the storaged energy is discharged to the load.

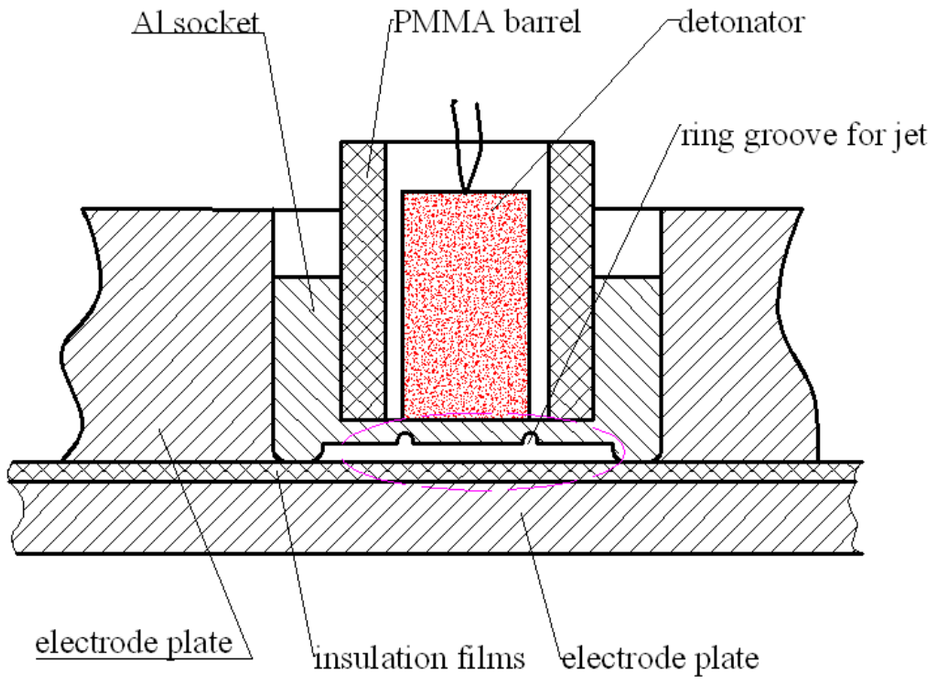

Fig. 6. Diagram of detonator switch

Fig. 7 shows the photoes of two apparatuses and Table 1 gives the electrical parameters of these two apparatuses.

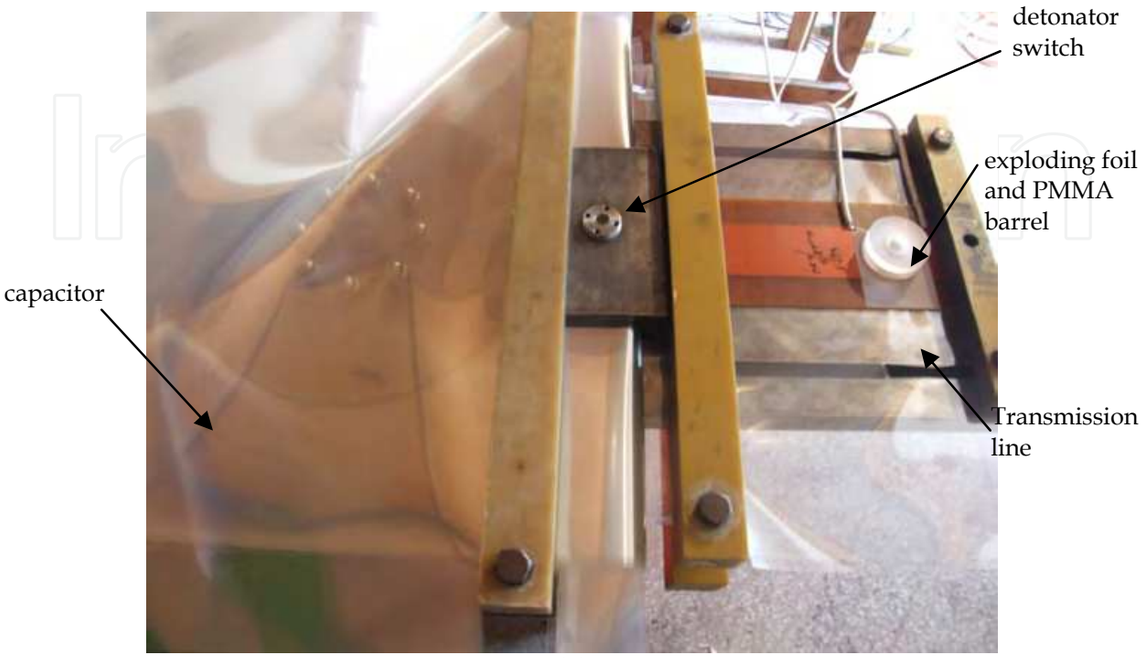

(a)

(b)

Fig. 7. Experimental apparatuses of metallic foil electrically exploding driving flyers. The apparatus with energy of 14.4 kJ (a) and the apparatus with energy of 40 kJ(b).

setup	C/μF	U_0/kV	E/kJ	R/mΩ	L/nH	T/μs	$(dI/dt)_{t=0}$ /(A/s)	Remarks
1	32	30	14.4	14	40	7.1	7.5×10^{11}	Single capacitor
2	32	50	40	10	36	6.75	8.4×10^{11}	Two capacitors in parallel

Table 1. Parameter Values of our two apparatuses

Table 2 gives the performance parameters of our two apparatuses of metallic foil electrically exploding driving flyers.

Parameters	Setup	
	1	2
Flyer—Mylar	ϕ(6～20)mm×(0.1～0.2)mm	ϕ(10～30)mm×(0.1～0.3)mm
Foil—Aluminum	(6～20)mm×(6～20)mm×0.028 mm	(10～30)mm×(10～30)mm×0.05 mm
Barrel—PMMA	ϕ(6～20)mm×(4～15)mm	ϕ(10～30)mm×(4～15)mm
Flyer velocity	3～10km/s	3～15km/s
Flyer Simultaneity at Impact	≤25 ns	≤35 ns

Table 2. The performance parameters of our two apparatuses

The typical velocity histories of the flyers are shown in Fig.8, which are measured by laser interferometer, such as VISAR (velocity interferometer system for any reflectors)[27] or DISAR(all fibers displace interferometer system for any reflectors)[28].

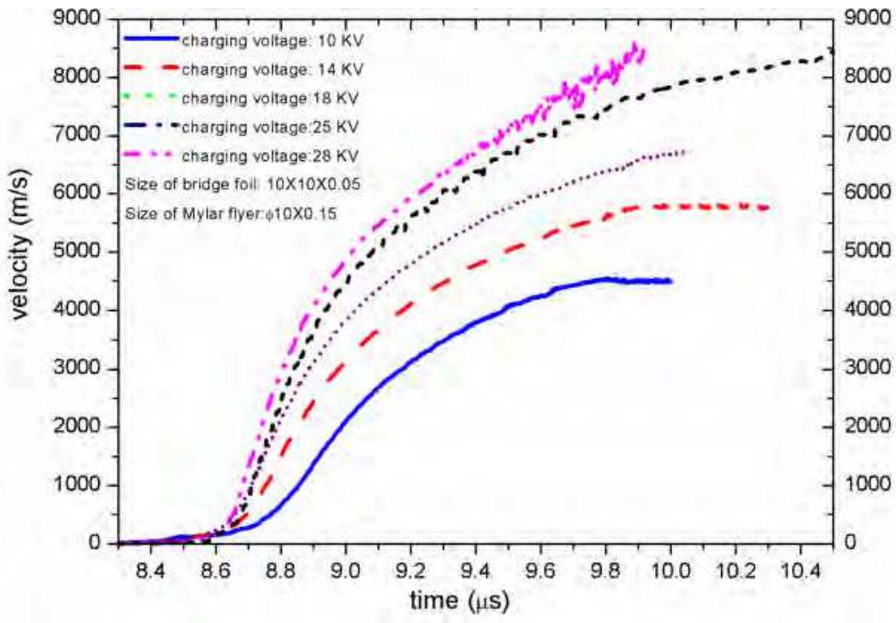

(a)

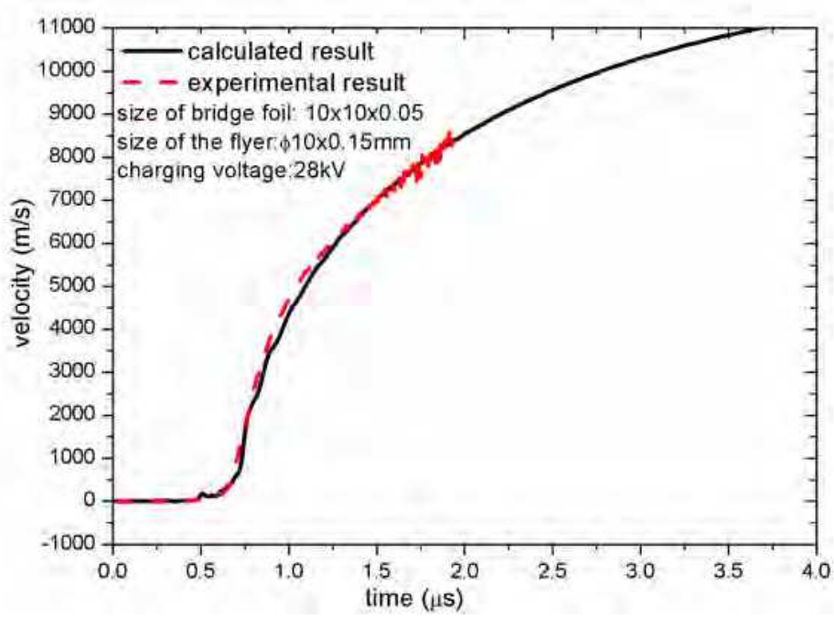

(b)

Fig. 8. The experimental results of the velocity of the flyer in different conditions. The velocities of the flyers vary from charging voltages (a) and the calculated and measured velocities of the flyers (b)

As described above, the apparatus of metallic foil electrically exploding driving flyers is a good plane wave generator for shock wave physics experiments. In the last part, we will introduce some important applications of this tool.

3.2 Magnetically driven quasi-isentropic compression

The techinques to realize magnetically driven quasi-isentropic compression are based on all kinds of pulsed power generators, such as ZR, Veloce[29], Saturn[30] facilities. As shown in Fig.9, Current $\vec{J}$ flowing at the anode and cathode surfaces induces a magnetic field $\vec{B}$ in

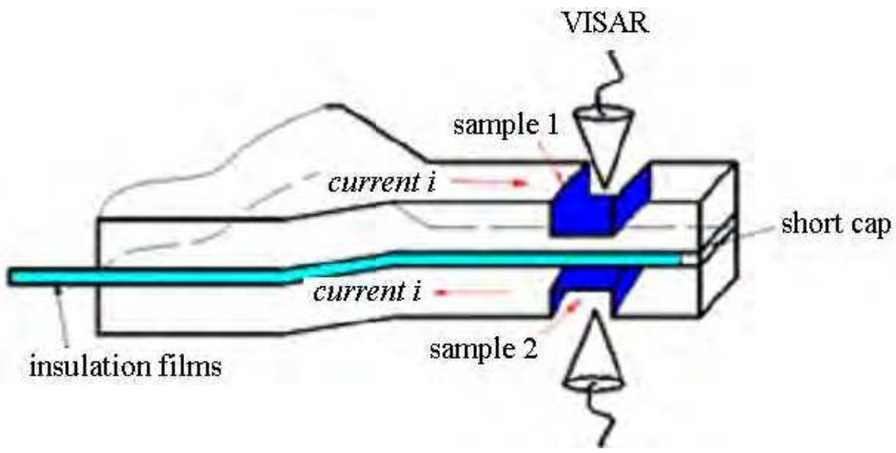

Fig. 9. Experimental configuration of samples for magnetically driven quasi-isentropic compression

the gap. The resulting $\vec{J} \times \vec{B}$ Lorentz force is transferred to the electrode material, and a ramp stress wave propagates into the samples. The stress normal to the inside surfaces of electrods is $P_B = (1/2)\mu_0 J^2$, where J is the current per unit width. Two identical samples with a difference in thickness of h, are compressed by identical B-force and their particle velocity profiles $u(t)$ are measured by DISAR or VISAR.

An inverse analysis technique, i.e, the backward integration technique using difference calculation is developed to extract a compression isentrope from free-surface or window-interface velocity profiles[31]. Different from Lagrangian wave analysis, inverse analysis can account for ramp-wave interactions that arise at free surfaces or window interfaces. In this method, the profiles of velocity and density are specified as an initial condition at the Lagrangian position of the measurement, then the equations of motion from equation (5) through equation (7) are integrated in the negative spatial direction to a position inside the material that is free of interaction effects during the time of interest. Assuming some parametric form shown in equation (8) for the mechanical isentrope of the material such as Murnaghan euqation or others, the parameter values are found by iteratively performing backward intergration on data from multiple thickness of the sample while minimizing the deviation between the results at a common position.

$$\sigma(h - \mathrm{d}h, t) = \sigma(h.t) + \rho_0[u(h, t + \mathrm{d}t) - u(h, t - \mathrm{d}t)]\mathrm{d}h / (2\mathrm{d}t) \tag{5}$$

$$\varepsilon(h - \mathrm{d}h, t) = F[\sigma(h - \mathrm{d}h), t)] \tag{6}$$

$$u(h - \mathrm{d}h, t) = u(h, t) + [\varepsilon(h, t + \mathrm{d}t) - \varepsilon(h, t - \mathrm{d}t)]\mathrm{d}h / (2\mathrm{d}t) \tag{7}$$

$$B_s(V) = B_{s0}\left(\frac{V_0}{V}\right)^{B'} \tag{8}$$

In order to do quasi-isentropic compression experiments, a compact capacitor bank facility CQ-1.5[13] was developed by us, which can produce a pulsed current with peak value of about 1.5 MA and rising time of 500 ns∼800 ns. The solid insulating films are used to insulate the anode electrode plates from the cathode ones. And the facility is used in the air. Fig.10 presents the picture of CQ-1.5.Based on CQ-1.5, about 50 GPa pressure is produced on the surface of steel samples. The parameter values of CQ-1.5 is given in Table 3.

performance parameters	values
total capacitance	15.88 μF
period in short-circuit	3.40 μs
rise time	500∼800 ns
total inductance	about 18 nH
total resistance	∼10 mΩ
charging voltage	75 kV∼80 kV
peak current	≥1.5 MA

Table 3. The specifications of CQ-1.5

(a) (b)

Fig. 10. The picture of experimental apparatus CQ-1.5 (a) and its load area including sample and measuring probe (b).

Fig. 11. shows the typical loading pressure histories. The pressure is a ramp wave.

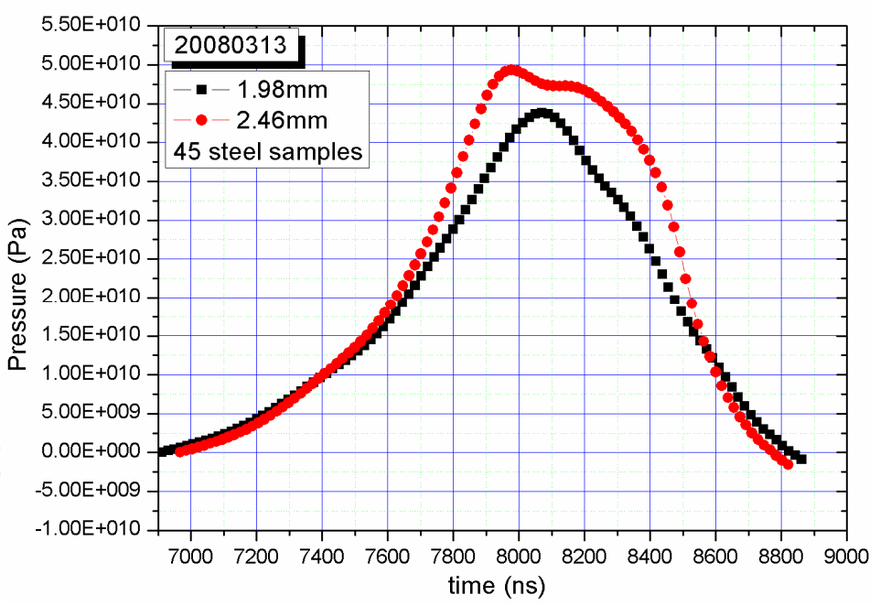

Fig. 11. The loading pressure histories of CQ-1.5

4. MHD simulation of metallic foil electrically exploding driving highvelocity flyers and magnetically driven quasi-isentropic compression

4.1 Metallic foil electrically exploding driving highvelocity flyers

The code used to simulate the electrical explosion of metallic foil is improved based our SSS code[32], which is one dimensional hydrodynamic difference code based on Lagrange orthogonal coordinate. For the case of electrical explosion of metallic foil, the power of Joule

heating is increase into the energy equation, and the magnetic pressure part is considered. In order to calculate the power of Joule heating and magnetic pressure, the discharging current history is needed which is detemined by the electric circuit equation (2) and equation (3). The resistance of foil varies from different phase states during dicharging process, so a precisionly electrical resistivity model is needed to decribe this change. The physical model is seen in Figure 1, and the Lagrange hydrodynamic equations are:

$$\begin{cases} V = \dfrac{\partial X}{\partial M} \\ \dfrac{\partial U}{\partial t} = -\dfrac{\partial \sigma}{\partial M} + f_{EM} \\ \dfrac{\partial E}{\partial t} = -\dfrac{\partial (\sigma U)}{\partial M} + \dfrac{\partial (\Delta P)}{\partial M} + \lambda \dfrac{\partial}{\partial M}\left(\dfrac{\partial T}{\partial X}\right) \\ \Delta P = I^2 R_{foil} \\ f_{EM} = \vec{j}(X) \times \vec{B}(X) / M \end{cases} \tag{9}$$

Where, V is specific volume, M is mass, X is Lagrange coordinate, U is velocity, T is temperature, λ is thermal conductivity, σ is the total pressure and $\sigma=p+q$, p is heating pressure, q is artifical viscosity pressure, f_{EM} is magnetic pressure per mass, E is total specific energy and $E=e+0.5U^2$, e is specific internal energy, ΔP is power of Joule heating, B is magnetic flux density, μ is vacuum permeability, k is shape factor and $k=0.65$, R_{foil} is resistance of metallic foil and I is the current flowing through metallic foil in the circuit, which can be expressed with equation (10).

$$\begin{cases} \dfrac{1}{C_0}\displaystyle\int_0^t I(t)dt + RI + L\frac{dI}{dt} = Vol_0 \\ L = L_s + L_d \\ R = R_s + R_{foil} \\ L_d = L(h+\Delta h) - L(h) = \dfrac{\mu l}{2\pi} \ln \dfrac{h + 1.23b}{h + \Delta h + 1.23b} \\ R_{foil}(t) = \dfrac{l}{b} \cdot \dfrac{1}{\displaystyle\int_0^h 1 \Big/ \eta(X,t)^{dX}} \end{cases} \tag{10}$$

In the equation (10), C_0 is the capacitance of the experimental device, L is the total inductance of the circuit, L_s is the fixed inductance of the circuit, L_d is the variable inductance of the expansion of metallic foil caused by electrical explosion, R is the total resistance of the circuit, and R_s is the fixed resistance and R_{foil} is the dynamic resistance of the foil caused by electrical explosion, b,h and l is the width, thickness and length of the foil, η is the electrical resistivity, which is variable and can be expressed by the model put

forward by T.J. Burgess[33]. The Burgess's model can describe the electrical resistivity of the foil at different phase states.
For solid state, there is

$$\eta_s = (C_1 + C_2 T^{C_3}) \cdot \left(\frac{V}{V_0}\right)^{F(\gamma)} \tag{11}$$

In equation (11), C_1, C_2 and C_3 are fitting constants, γ is Gruneisen coefficient, for many materials ,F(γ)=2γ-1.
For liquid state, there is

$$\eta_L = \Delta\eta \cdot (\eta_s)_{T_m} \cdot \left(\frac{T}{T_m}\right)^{C_4} \tag{12}$$

In equation (12), for many materials, $\Delta\eta = ke^{0.069 L_F / T_m}$, k is a constant, L_F is the melting latent heat, T_m is melting point temperature and C_4 is fitting constant.
For gas state, the electrical resistivity is related with both the impact between electrons and ions and between electrons and neutrons. so,

$$\begin{cases} \eta_v = \eta_{ei} + \eta_{en} \\ \eta_{ei} = \dfrac{C_5}{T}[1 + \ln(1 + C_6 V T^{3/2}) \\ \eta = C_7 T^{1/2}[1 + \alpha_i^{-1}] \\ \partial_i = (1 + \dfrac{C_8 e^{C_9/T}}{VT^{3/2}})^{-1/2} \end{cases} \tag{13}$$

In equation (13), α_i is the ionization fraction, C_5, C_6 , C_7, C_8 and C_9 are fitting constants.
In fact, there is mixed phase zone between liquid and gas states, a mass fraction m is defined. When m=0, all mass is condensed, and m=1, all mass is gas, and 0<m<1, the mass is mixture states. Two mixture variants are also defined besides mass fraction.

$$\begin{cases} m = (V - V_0)\dfrac{C_{10}}{C_{11}} e^{-C_{12}/T} \\ X_c = (1 - m) / (V / V_0) \\ X_V = 1 - X_C \end{cases} \tag{15}$$

Where C_{10}, C_{11} and C_{12} are fitting constants.
The electrical resistivity of mixed phase zone can be expressed

$$\begin{cases} \eta_{mixed} = \left(\dfrac{X_C}{\eta_c} + \dfrac{X_V}{\eta_V}\right)^{-1} \\ \eta_c = \eta_l \end{cases} \tag{16}$$

Table 4 gives the parameters values of Burgess's model for Aluminum, which is used in our experiments.

C_1(mΩ-cm)	C_2	C_3	C_4	C_5	C_6	γ_0	L_F(Mbar-cm^3/mole
-5.35e-5	0.233	1.210	0.638	1.5	1.20e-2	2.13	0.107
C_7	C_8	C_9	C_{10}	C_{11}	C_{12}	k	$T_{m,0}$ (ev)
3.80e-3	18.5	5.96	0.440	3.58e-2	3.05	0.878	0.0804

Table 4. The parameters values of Burgess's model for Aluminum

The calculated results are presented in from Fig.12 through Fig.15. In Fig.14 and Fig.15, the experimental and calculated results are compared.

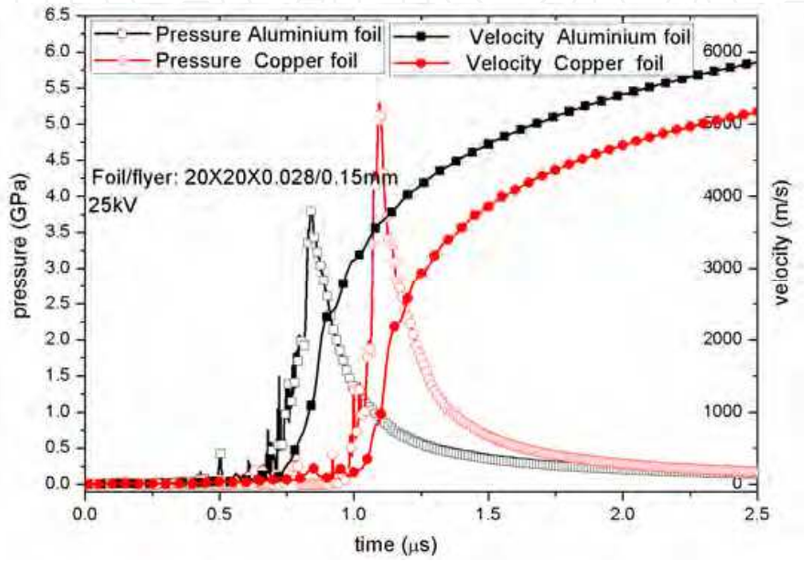

Fig. 12. The calculated pressure and flyer velocity history results of electrical explosion of Aluminum and Copper foils.

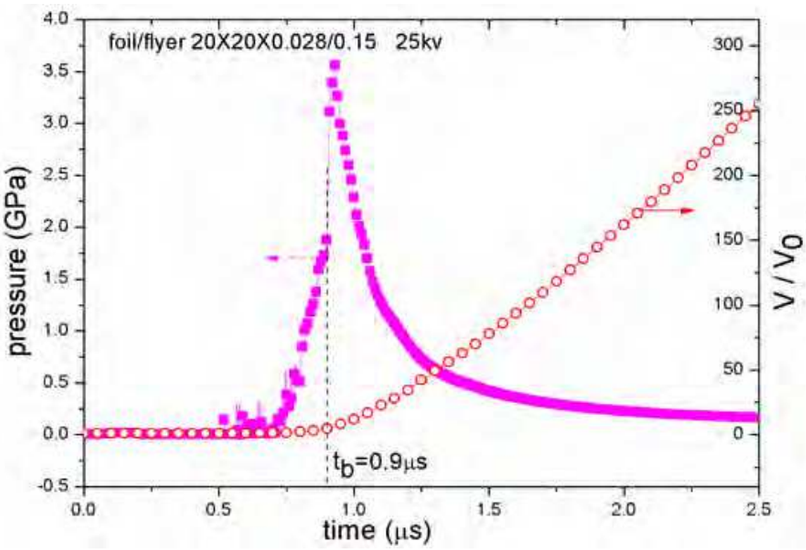

Fig. 13. The calculated results of pressure and specific volume of aluminum foil when exploding.

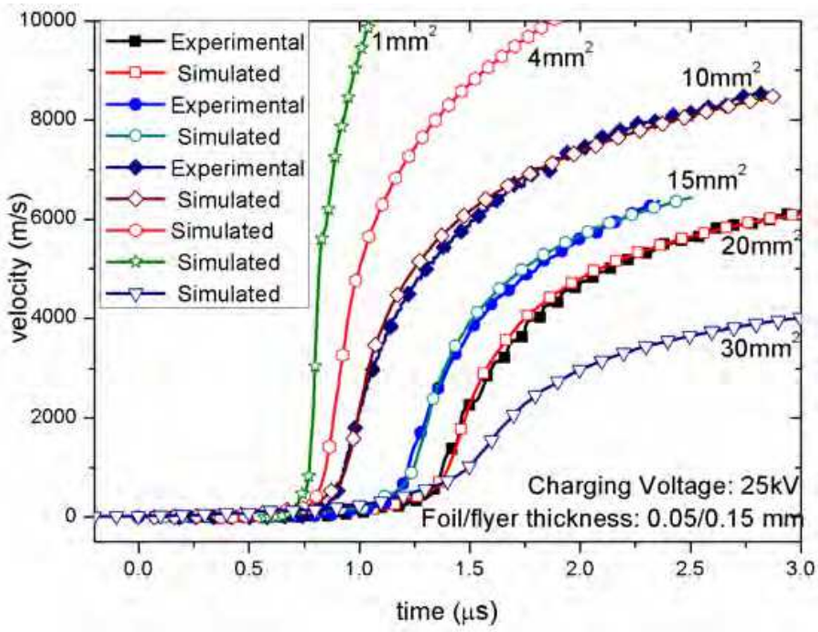

Fig. 14. The calculated and experimental results of flyer velocities for different flyer sizes.

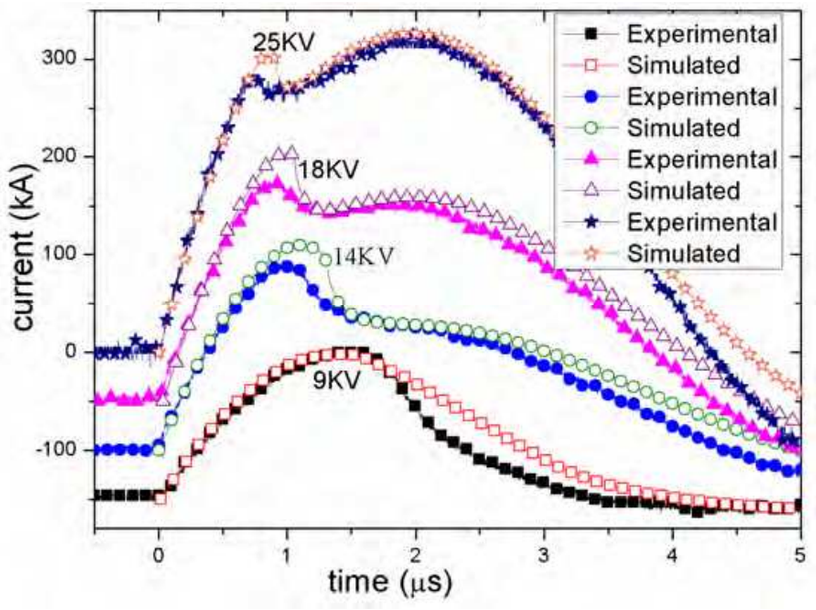

Fig. 15. The experimental and calculated results of discharging current.

The results presented in Fig.12 through Fig.15 show that the physical model here is appropriate to the electrical explosion of metallic foils.

4.2 Magnetically driven quasi-isentropic compression

In order to simplify the problem, the one dimensional model of magnetically driven quasi-isentropic compression can be described by the model shown in Fig.16. The changes of

electrical parameters caused by the motion of loaded electrode are not considered, and the heat conduction is neglected because it is slow in sub microsecond or one microsecond. A standardly discharging current in short circuit is as input condition presented in Fig.17. The relative magnetic permeability is supposed tobe 1, that is to say , $\mu \cong \mu_0$.

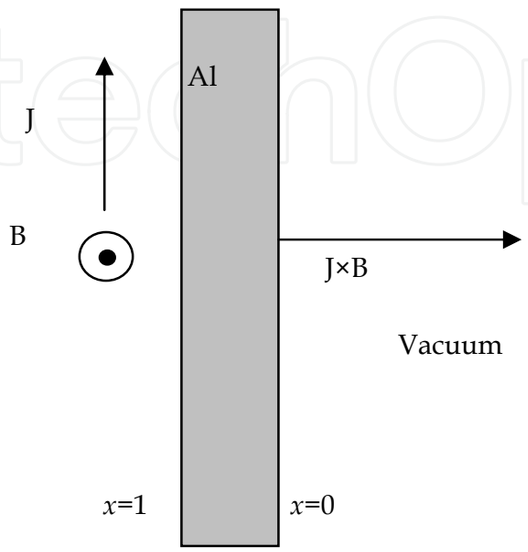

Fig. 16. Physical model of simulation

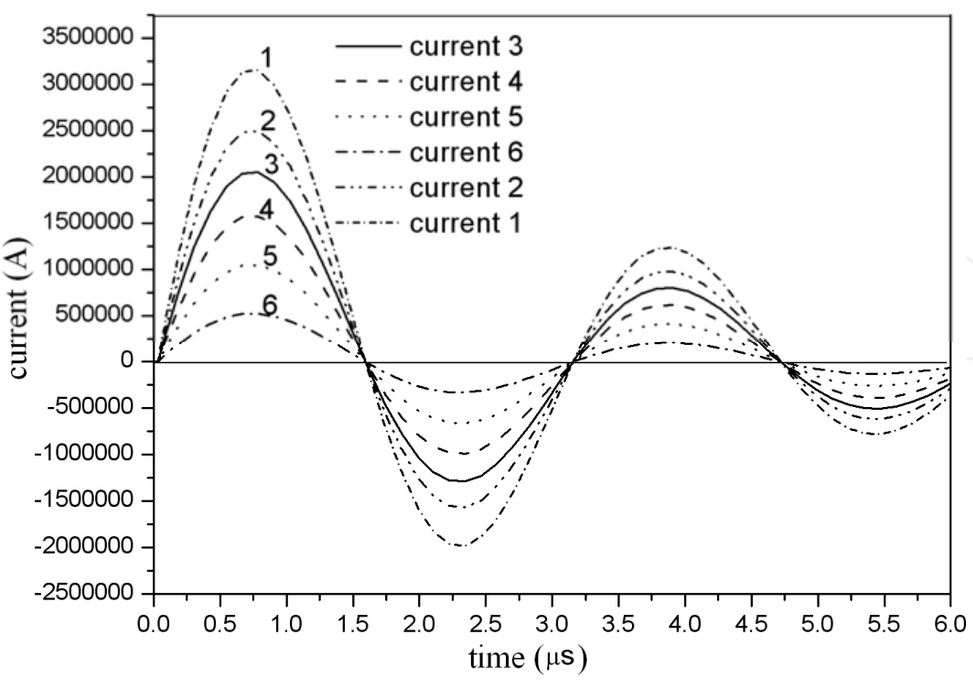

Fig. 17. Loading current curves

The controlling equations are one dimensionally magnetohydrodynamic ones, which include mass conservation equation, momentum conservation equation, energy conservation equation and magnetic diffusion equation, as shown in equation (4). The original boundary conditions are,

For t=0 , $\begin{cases} x=0:B=0,P=0 \\ x=1:B=0,P=0 \end{cases}$, and for t=t_{n}（at some time）, $\begin{cases} x=0:B=0,P=0 \\ x=1:B=\mu_0 J(t),P=0 \end{cases}$.

The calculation coordinate are Lagrangian ones, and for the Lagrangian coordinate, the equation (4) can be converted to equations from (17) through (19).

$$\rho_0 \frac{du}{dt} + \frac{\partial}{\partial x}\left(p + q + \frac{B^2}{2\mu_0} \right) = 0 \tag{17}$$

$$\rho_0 \frac{de}{dt} + (p+q)\frac{dV}{dt} - \rho_0 \dot{e}_D = 0 \tag{18}$$

$$\frac{\partial (VB)}{\partial t} = \frac{\partial}{\partial x}\left[\frac{\eta}{\mu_0 B}\frac{\partial (VB)}{\partial x} \right] \tag{19}$$

The equation of electrical resistivity is also very important for the case of magnetically driven quasi-isentropic compression. In order to simplify the problem, a simple model is considered.

$$\eta = \eta_0 (1 + \beta Q) \tag{20}$$

In equation (20),η_0 is the electrical resistivity of conductors at temperatureof 0 °C,β is heating factor, Q is the heat capacity or increment of internal energy relative to that at temperatureof 0 °C, which is related with temprature at the condensed states.

$$Q = c_{\mathrm{v}} T \tag{21}$$

In equation (21), c_{v} is specific heat at constant volume, which is close to constant from 0 °C to the temperature of vaporazation point.

For aluminum, β is 0.69×10^{-9} $\mathrm{m^3/J}$, η_0 is 2.55×10^{-8} Ωm. Before vaporazation point, the equation (20) is suitable. After that, more complex electrical resisistivity model is needed.

In this simulation, the stress wave front is defined when the amplitude of pressure reaches to 0.1 GPa, and thediffusion front of magnetic field is determined when the magnetic flux density is up to 0.2 T[34]。

Fig.18 gives the distribution of density and temperature of Aluminum sample along Lagrangian coordinates for different times in the condition of loading current density 1.5 MA/cm.

The results in Fig.18 show that the density and temperature of aluminum sample vary with the loading time along the direction of sample thickness because of the Joule heating and magnetic field diffusion.

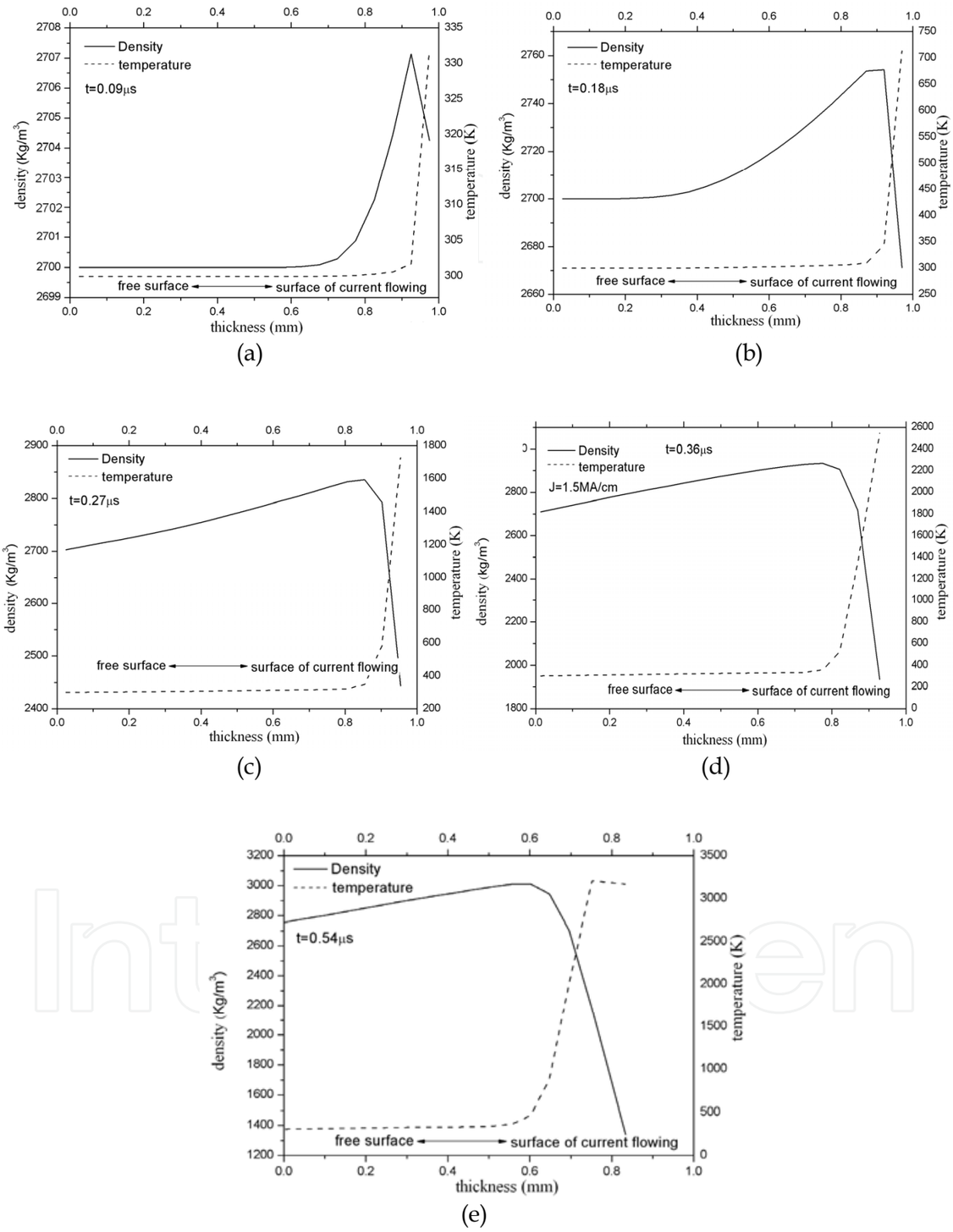

Fig. 18. Distribution of density and temperature of Aluminum sample along Lagrangian coordinates for different times under the condition of loading current density 1.5 MA/cm at time of 0.09 μs (a), 0.18 μs (b), 0.27 μs (c), 0.36 μs (d) and 0.54 μs (e)

Fig.19 gives the calculated results of distribution of magnetic induction strength along Lagrangian coordinates for different times in the condition of loading current density 1.5MA/cm.

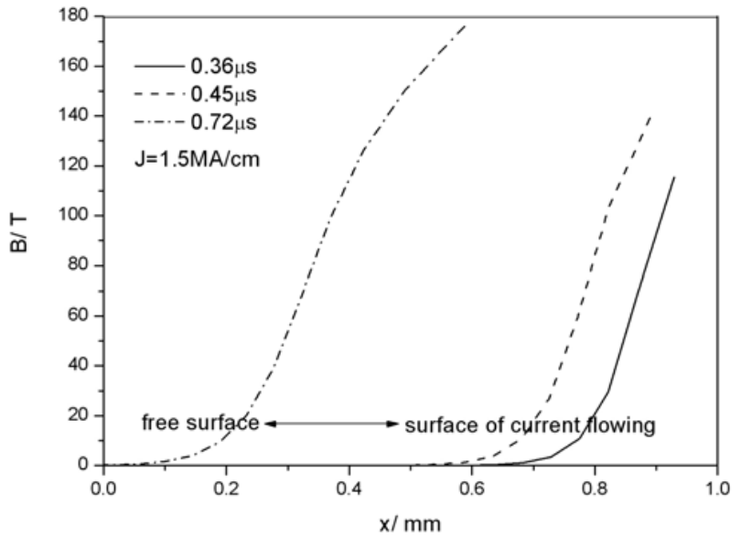

Fig. 19. Distribution of magnetic induction strength along Lagrangian coordinates for different times in the condition of loading current density 1.5MA/cm

And Fig.20 gives the physical characteristics of hydrodynamic stress wave front and magnetic diffusion front under the Lagrangian coordinates. The velocity of stress wave front is far more than that of the magnetic diffusion front, which is the prerequisite of magnetically driven quasi-isentropic compression. And the velocity of magnetic diffusion front increases gradually with the increasing of loading current density.

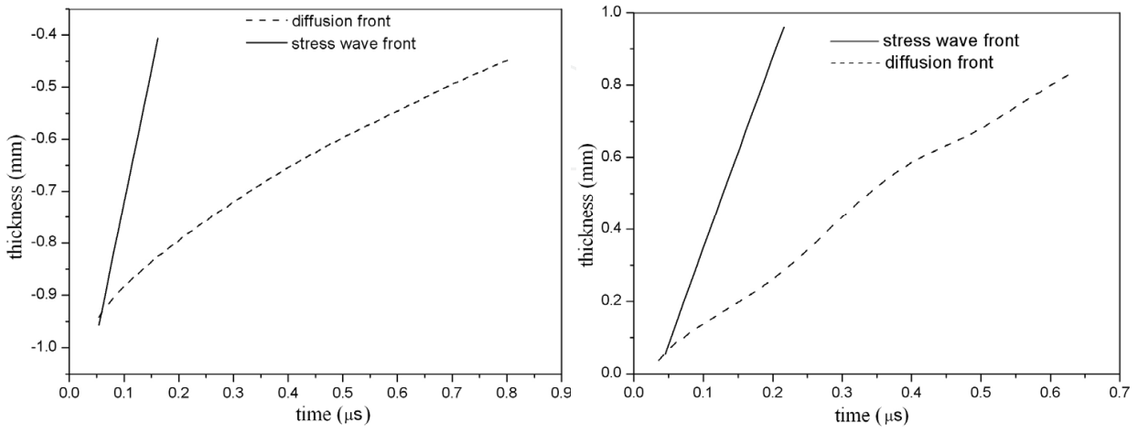

(a) current density of 1MA/cm (b) current density of 3MA/cm

Fig. 20. Physical characteristics of hydrodynamic stress wave front and magnetic diffusion front under the Lagrangian coordinates

Fig.21 presents the relationships between the velocity of magnetic diffusion front and loading current density. The results show that an inflection poin occurs at the loading current density of 1 MA/cm, and that the results can be expressed with two linear equations (22)

$$\begin{cases} D = 0.008 + 0.46J, & 1.0 < J \le 3 \ \ \mathrm{MA/cm} \\ D = 0.36 + 0.06J, & 0.5 \le J \le 1.0 \ \ \mathrm{MA/cm} \end{cases} \tag{22}$$

In equation (22), D is the velocity of magnetic diffusion, and J is loading current density.

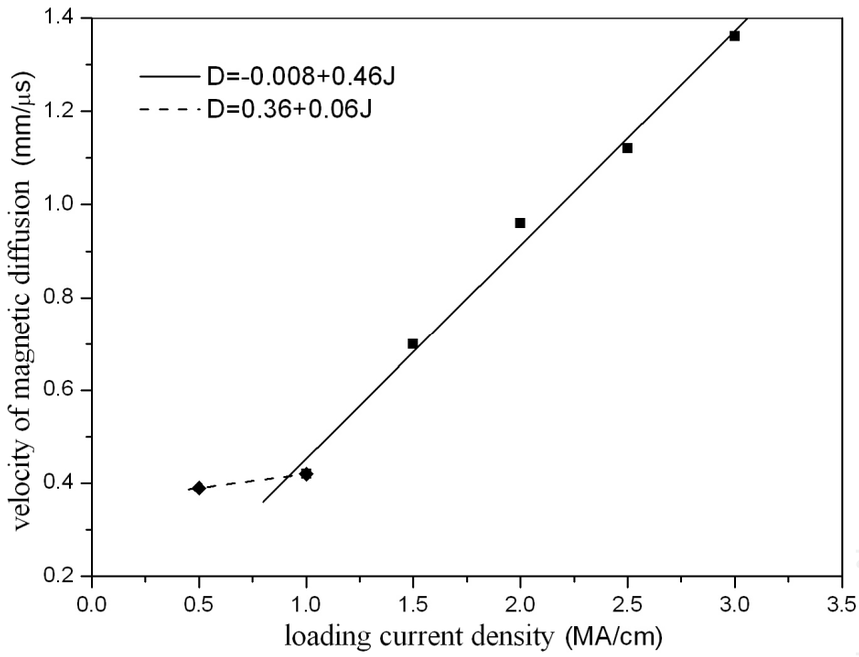

Fig. 21. The relationship of magnetic diffusion velocity varying with loading current densities.

Fig.22 is the case of copper samples under magnetically driven quasi-isentropic compression. The calculated results show that the particle velocity curves become steeper with the increasing of sample thickness, and that the shock is formed when the thickness is more than 2.5 mm for this simulating condition.

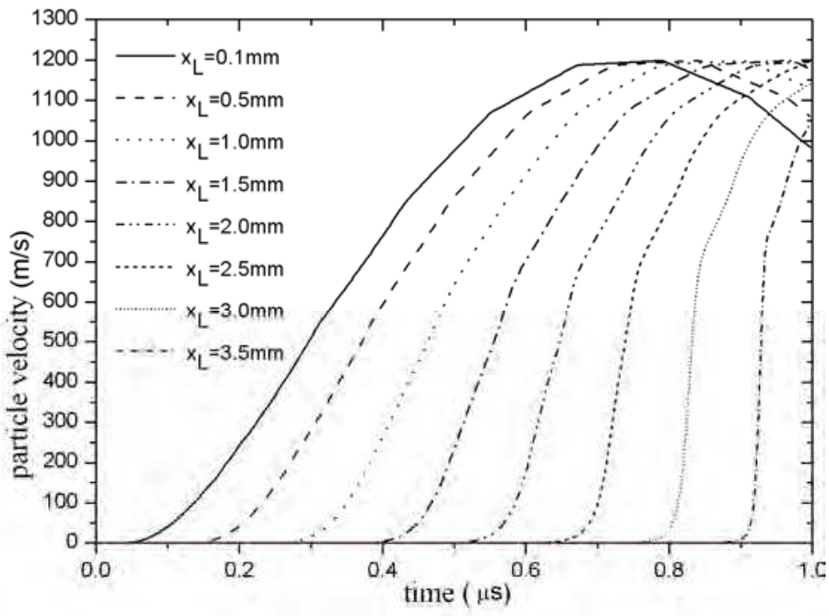

Fig. 22. The particle velocities of copper sample at different thickness in the condition of loading current density of 3 MA/cm.

5. Applications of metallic foil electrically exploding driving highvelocity flyers and magnetically driven quasi-isentropic compression

5.1 Metallic foil electrically exploding driving highvelocity flyers

5.1.1 Short-pulse shock initiation of explosive

The apparatus of metallic foil electrically exploding driving high velocity flyer offers an attractive means of performing shock initiation experiments. And the impact of an electrically exploding driven flyer produces a well-defined stimulus whose intensity and duration can be independently varied. Experiments are low-cost and there is fast turn-around between experiments.

Short-pulse shock initiation experiments will be very useful in developing more realistic theoretical shock initiation models. For the present, the models predicting shock initiation thresholds is short of, where very short pulses are employed . The technique can provide data to test the capability of improved models.

Based on our experimental apparatus, the shock initiation characteristics of TATB and TATB-based explosives are studied[35,36]. Fig.23 and Fig.24 show the experimental results of shock initiation thresholds and run distance to detonation of a TATB-based explosive.

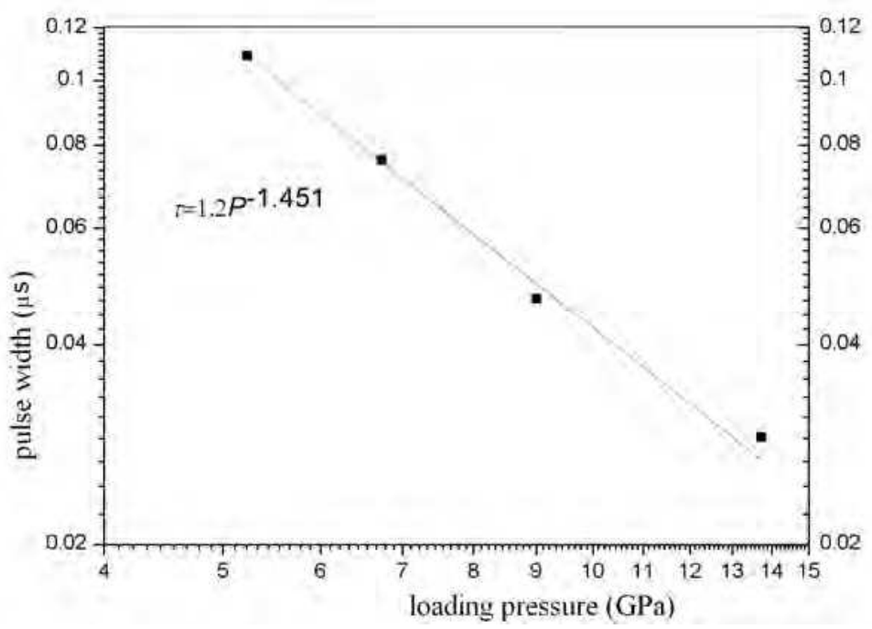

Fig. 23. Shock initiation threshold of 50% probability of initiation

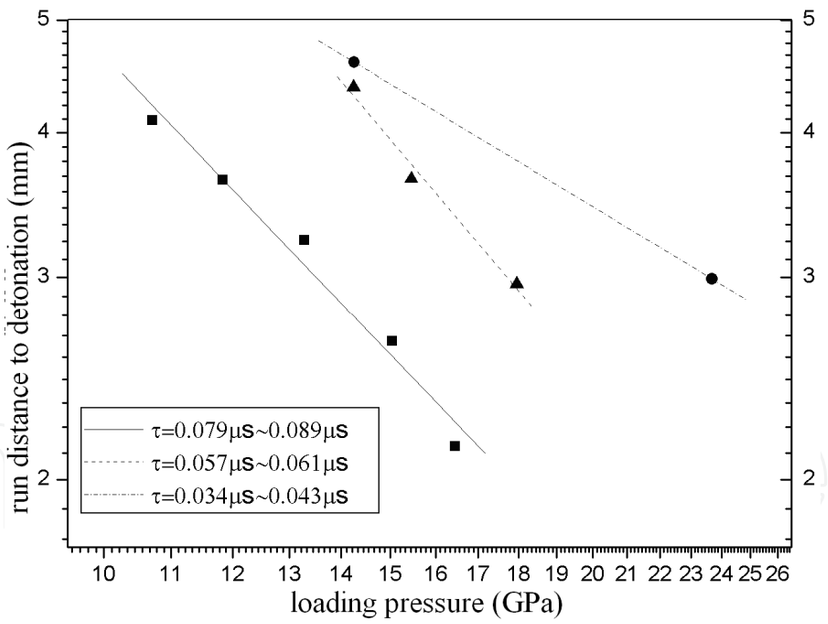

Fig. 24. Run distance to detonation in a TATB-based explosive

These experiments have the additional advantage of being applicable to relatively small explosive samples, an important consideration for evaluating and ranking new explosives.

5.1.2 Spallation experiments of materials

Compared with gas gun and explosively driven loading, The apparatus of metallic foil electrically exploding driving high velocity flyer is also a good tool used to research

dynamic behaviors of materials. The loading strain rates and stress duration vary easily. In order to study damage properties of materials using the apparatus of metallic foil electrically exploding driving high velocity flyer, a concept of two-stage flyer is put forward[37]. The Mylar flyer flies some distance to impact a buffer plate such as PMMA or nylon with different thickness, and the pressure produced in the buffer is attenuated to the expected value, and then the attenuated pressure propels the impactor on the buffer to some velocity to impact the target. The impactor is the same material as the target. Fig.25 is the diagram of the two-stage flyer based on the apparatus of metallic foil electrically exploding driving high velocity flyer.

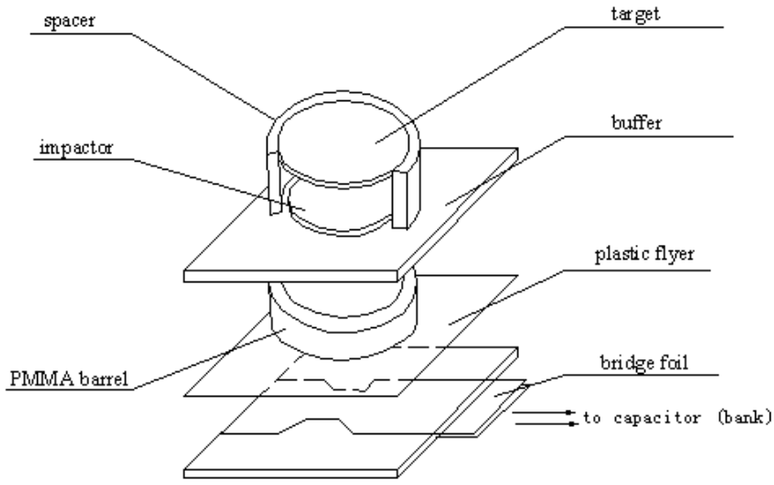

Fig. 25. Sketch of two-stage flyer based on the apparatus of metallic foil electrically exploding driving high velocity flyer

By means of the two-stage flyer, the spallations of steel and copper samples were researched. Fig.26 is the experimental results[38].

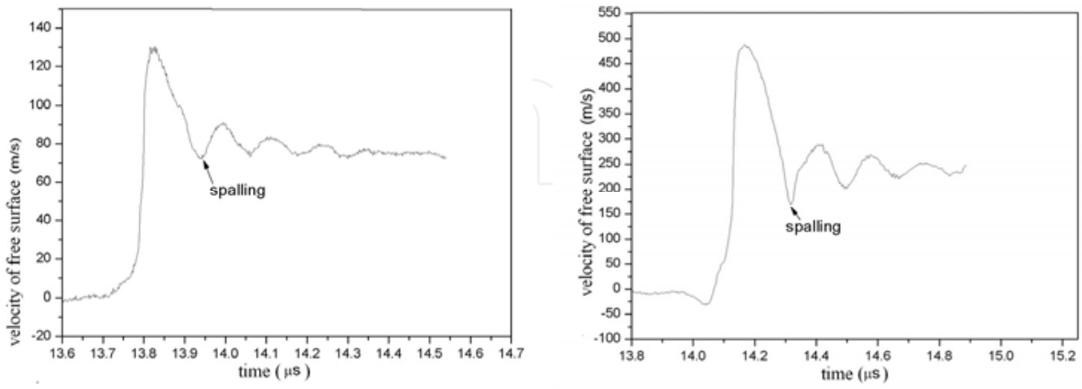

(a) (b)

Fig. 26. Experimental results of spallation , steel target (a) and copper target (b).

It is also convenient to study other dynamic behaviors of materials using the electric gun. Further experimental researches about materials are being done by our research group.

5.1.3 Potential applications

Equation of state (EOS) measurement is an important potential application for our apparatus. In order to increase the loading pressure of this apparatus, two improvements should be done. Firstly, the flyer should be Mylar-metal foil laminate flyer . The metal layer increases the flyer's shock impedance and thus the pressure produced in the target. Secondly, the storaged energy of apparatus should be increased. The expected pressure should be up to 200 GPa or more.

Impact experiment on the structure is also an important application for the apparatus of metallic foil electrically exploding driving high velocity flyer. For the apparatus of metallic foil electrically exploding driving high velocity flyer, its environment is well-controlled and instrumented, so it is suitable for studying impact phenomena in the fields of space science. Fig.27 shows a result of flyer of our apparatus impacting multi-layer structure.

Fig. 27. Experimental result of flyer impact multi-layer structure

5.2 Magnetically driven quasi-isentropic compression

5.2.1 Compression isentropes of copper and aluminum

The experimental compression isentropes of T1 copper andL1 pure aluminum(Al content more than 99.7%) were measured on the CQ-1.5. The free-surface velocities were measured by DISAR, and the data were processed with the backward integration code developed by us. For the design of sample sizes, it is necessary that shock should not be formed in the samples and the side rarefaction wave should not affect the center regime to meet the requirements of one dimensional strain loading. Table 5 are the sizes of experimental samples.

Exp. Shot.	materials	thickness		width
		$h1$	$h2$	w
20070605	T1 copper	2.00 mm	1.58 mm	7 mm
20070608-1	T1 copper	2.08 mm	1.78 mm	5 mm
20070608-2	T1 copper	2.04 mm	1.52 mm	7 mm
20070705	L1 aluminum	2.60 mm	2.02 mm	5 mm

Table 5. Experimental conditions

Fig.28(a) are the typical free-surface velocity histories measured by DISAR, which show that the slope become steeper for thicker sample. The experimental compression isentropes, theoretical compression isentropes and shock Hugoniots data are presented in Fig.28(b) and Fig.28 (c).

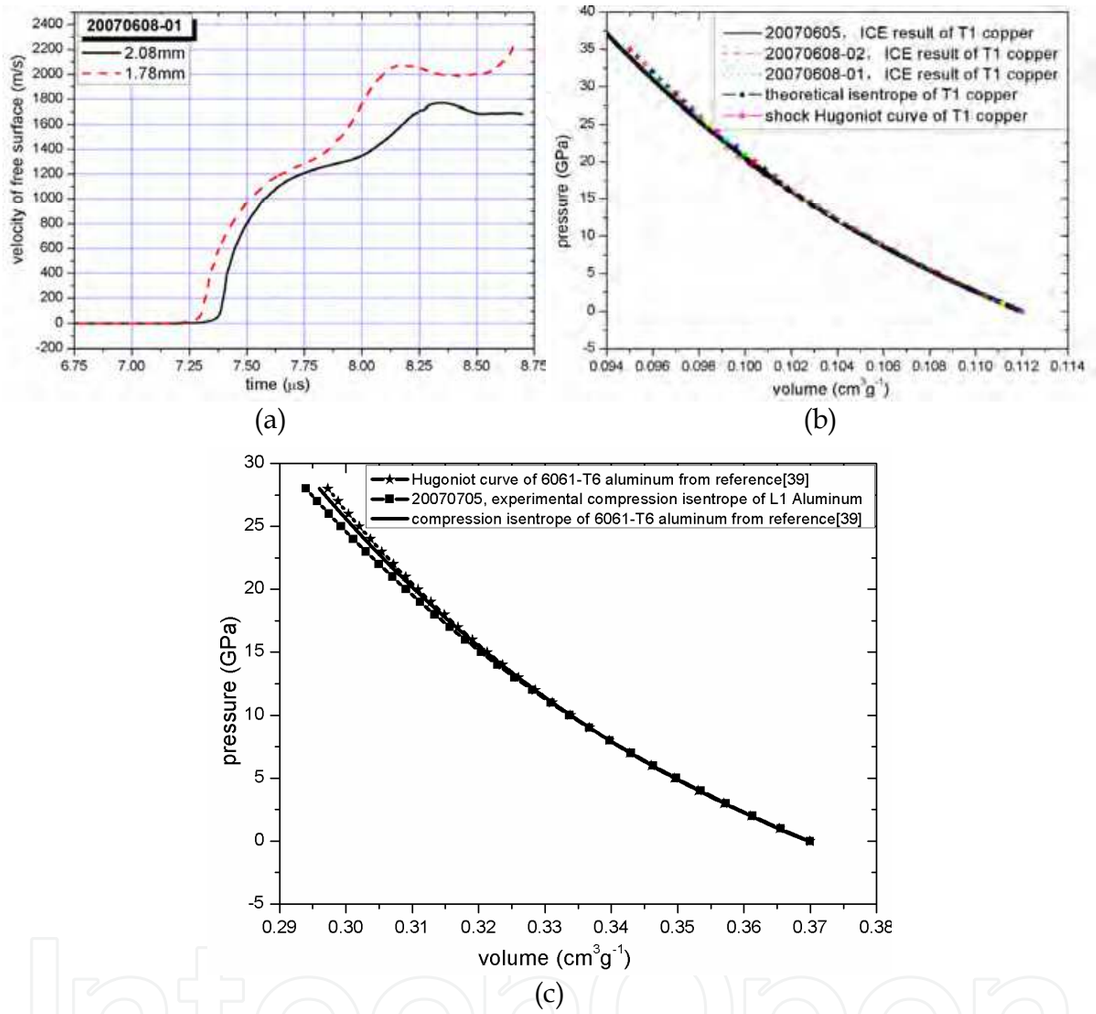

Fig. 28. Results of ICEs.(a) typical histories of free-surface velocity. (b) experimental, theoretical isentropes and Hugoniots data of T1 copper. (c) experimental isentrope of L1 pure aluminum, isentrope ang Hugoniot data of 6061-T6 aluminum from reference [39].

The results show that the experimental compression isentropes are consistent with the theoretical ones within a deviation of 3%, and are close to the shock Hugoniot data under the pressure of 40GPa and lies under them. Different from the shock method, the whole isentrope can be obtained in one shot, and tens of shots are needed to gain one shock Hugoniot curve. The calculation results[40] show that the compression isentropes gradually deviate from the shock Hugoniots with the increasement of loading pressure over 50 GPa. Therefore, the compression isentropes mainly reflect the off- Hugoniot properties of materials. Under 50 GPa, the compression isentropes are close to the shock Hugoniots, so we can use the isentrope data to check the validity or precision of shock Hugoniots.

5.2.2 Phase transition of 45 steel

Since the quasi-isentropic compression loading technique actually follows the *P-v* response of the material under investigation, the actual evolution of the phase trnasition can be observed. The classical polymorphic transtion of iron at 13 GPa has been studied under quasi-isentropic compression. The two free-surface velocity profiles recorded in our experiments are shown in Fig.28. The elastic precursor wave is clearly seen in the lower pressure region of the two profiles. And the plastic wave and phase change wave occur, which show that the polymorphic transition(α→ε) takes place. The velocity profiles in Fig.29 indicates that the onset of the phase transition is at velocity of 681 m/s, and the pressure of phase transition is also about 11.4 GPa.

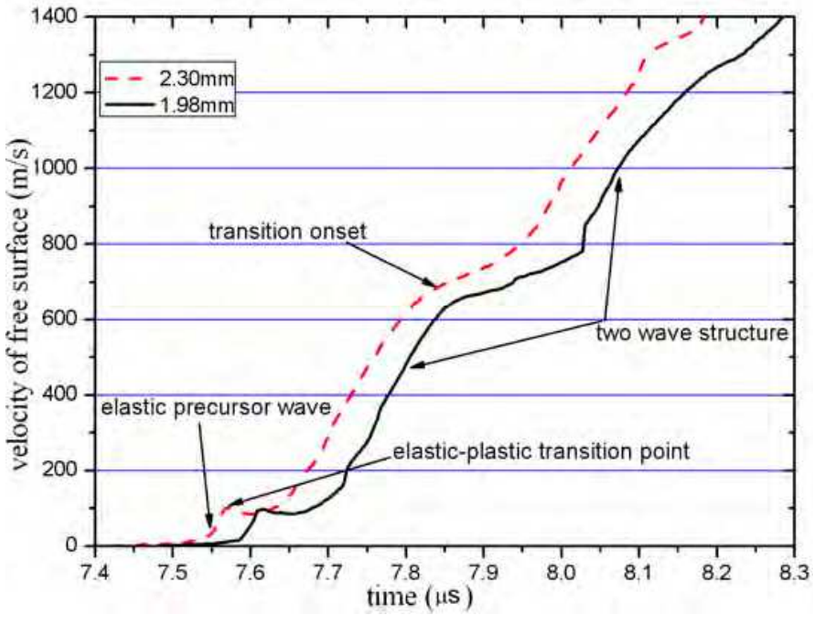

Fig. 29. Velocity profiles of 45 steel under quasi-isentropic compression

5.2.3 Spallation and elasto-plastic transition of pure tantalum

Fig.29 shows the results of the spalling experiments for pure tantalum (Ta contents 99.8%). The loading strain rate is 2.53×10^5 1/s. For the sample with thickness of 1.66 mm, the spallation is not obvious, perhaps the mirco-damage occurs. For the sample with thickness of 1.06 mm, the spallation is obvious, and the pull-back velocity is 129.6 m/s. According to the formular (23), the spall strength is 4.49 GPa.

$$\sigma_{\text{spall}} = \frac{1}{2}\rho_0 C_1 \Delta U_{\text{pb}} \tag{23}$$

where ρ_0 is the initial density of sample, C_l is the Larangian sound speed, ΔU_{pb} is the pull-back velocity as shown in Fig.4, and σ_{spall} is the spall strength of materials.

Under quasi-isentropic compression, the elasto-plastic transition are clearly shown in the velocity profiles of 45 steel and pure tantalum in Figure 28 and Fig.30. Here a concept of isentropic elastic limit(IEL, σ_{IEL}) is introduced. For the 45 steel sample, the σ_{IEL} is 2.26 GPa at the loading strain rate of 6.73×10^5 1/s, and for the pure tantalum sample, the σ_{IEL} is 2.42 GPa

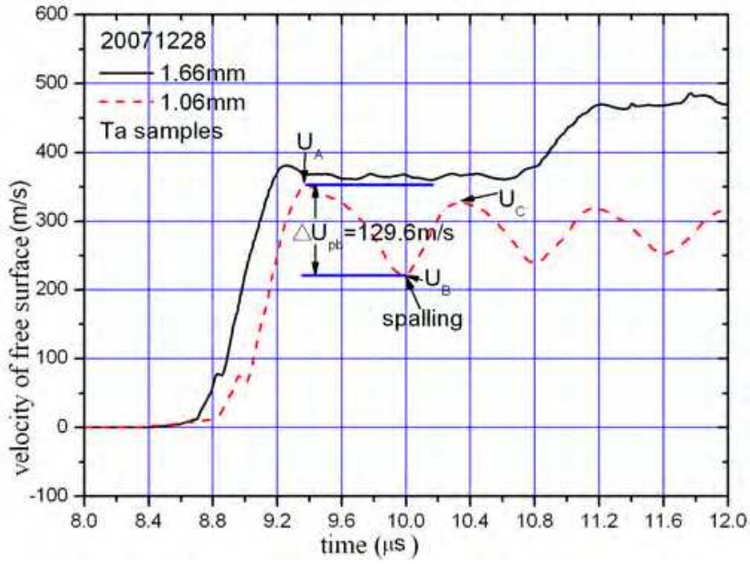

Fig. 30. Velocity profiles of Tantalum samples

at the loading strain rate of 2.53×10^5 1/s. Because of the difference of loading strain rates, the σ_{IEL} ranges from 2.26 to 2.35 GPa for 45 steel, and from 2.42 to 2.70 GPa for pure tantalum in our experiments, correspondingly, the yield strength ranges from 1.29 to 1.34 GPa for 45 steel and from 1.12 to 1.25 GPa for pure tantalum.

5.2.4 Magnetically driven high-velocity flyers

It is an important application to launch high-velocity flyer plates using the techniques of magnetically driven quasi-isentropic compression. For the present, the reseachers has launched the aluminum flyer plate with the size of 15 mm×11 mm×0.9 mm to the velocity of 43 km/s using this technique[23], and can produce 1～2 TPa shock pressure on the heavy metallic or quartz samples. Based on CQ-1.5, the aluminum flyer plate with the size of 8 mm×6 mm×0.9 mm was launched to about 9 km/s by us. Figure 31 shows the experimental results of the velocities of the flyers.

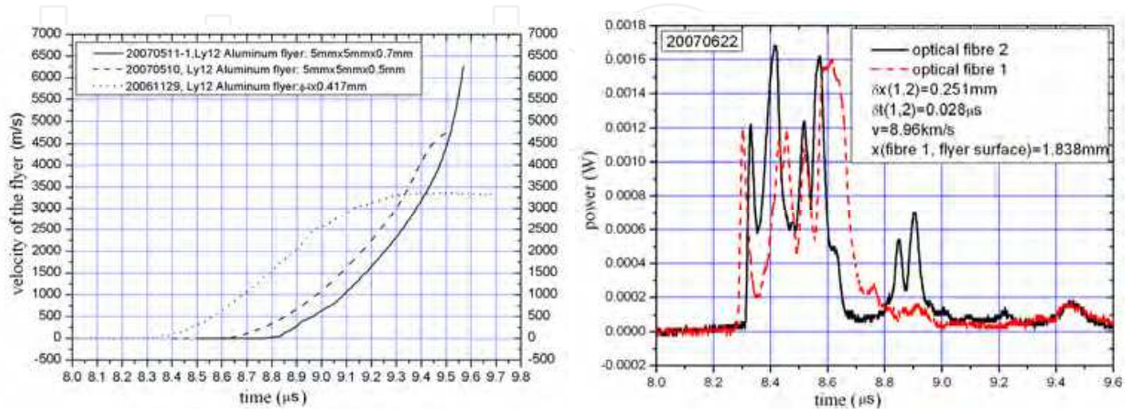

(a) (b)

Fig. 31. The velocities of the aluminum flyer plates driven by magnetic ressure.The velocities measured by VISAR (a) and the averaged velocity measured by optical fibres pins (b)

6. Summary

The physical processes of electrical explosion of metallic foil and magnetically driven quasi-isentropic compression are very complex. This chapter dicusses these problem simply from the aspect of one dimensionally magnetohydrodyamics. The key variable of electrical resistivity was simplified, which is very improtant. Especially for the problem of magnetically driven quasi-isentropic compression, only the resistivity is considered before the vaporazation point of the matter. In fact, the phase states of the loading surface vary from solid to liquid, gas and plasma when the loading current density becomes more and more. In order to optimize the structural shapes of electrodes and the suitable sizes of samples and windows in the experiments of magnetically driven quasi-isentropic compression, two dimensionally magnetohydrodynamic simulations are necessary.

The applications of the techniques of electrical explosion of metallic foil and magnetically driven quasi-isentropic compression are various, and the word of versatile tools can be used to describe them. In this chapter, only some applications are presented. More applications are being done by us, such as the quasi-isentropic compression experiments of un-reacted solid explosives, the researches of hypervelocity impact phenomena and shock Hugoniot of materials at highly loading strain rates of $10^5 \sim 10^7$ 1/s.

7. Acknowledgements

The authors of this chapter would like to acknowledge Prof. Chengwei Sun and Dr. Fuli Tan, Ms. Jia He, Mr. Jianjun Mo and Mr. Gang Wu for the good work and assistance in our simulation and expeimental work. We would also like to express our thanks to the referee for providing invaluable and useful suggestions. Of cousre, the work is supported National Natural Science Foundation of China under Contract NO. 10927201 and NO.11002130, and the Science Foundation of CAEP under Contract NO. 2010A0201006 and NO. 2011A0101001.

8. References

[1] Keller D. V. and Penning R. J., Exploding foils—the production of plane shock waves and the acceleration of thin plates, Exploding Wires, W. G. Chase and H. K. Moore, Eds. Plenum Press, New York,Vol.2. 1962: 263

[2] Guenther A. H. ,Wunsch D. C. and Soapes T. D., Acceleration of thin plates by exploding foil techniques, Exploding Wires, W. G. Chase and H. K. Moore, Eds. Plenum Press, New York, Vol.2. 1962: 279

[3] Kotov Y A, Samatov O. M., Production of nanometer-sized AlN powders by the exploding wire method[J]. Nanostructured Materials, Vol.12(1-4),1999: 119

[4] Suzuki T, Keawchai K, Jiang W H. Nanosize Al_2O_3 powder production by pulsed wire discharge[J]. Jpn, J. Appl. Phys., Vol.40, 2001: 1073

[5] Weingart R.C. , Electric gun: applications and potential, UCRL-52000-80-2,1980

[6] Steinberg D. , Chau H., Dittbenner G. et al, The electric gun: a new method for generating shock pressure in excess of 1 TPa, UCI-17943, Sep. 1978

[7] Weingart R.C.,Chau H.H., Goosman D.R. et al, The electric gun: A new tool for ultrahigh-pressure research, UCRL-52752, April 1979

[8] Sun Chengwei, Private Communications, 2004

[9] Hawke R. S., Duerre D. E., Huebel J. G. et al, Electrical Properties of Al_2O_3 under Isentropic Compression up to 500Gpa(5Mbar)[J]. J. Appl. Phys., Vol.49(6), June 1978: 3298～3303

[10] Asay J. R., Isentropic Compression Experiments on the Z Accelelator. Shock Compression of Condensed Matter-1999, Edited by M. D. Furnish, L.C. Chhabildas and R. S. Hixson, 2000: 261～266

[11] Avrillaud G., Courtois L., Guerre J. et al, GEPI: A Compact Pulsed Power Driver for Isentropic Compression Experiments and for Non Shocked High Velocity Flyer Plates. 14th IEEE Int·l Pulsed Power Conf., 2003: 913～916

[12] Rothman S. D., Parker K. W. et al, Isentropic compression of lead and lead alloy using the Z machine, Shock Compression of Condensed Matter – 2003, 1235-1238，2004

[13] Wang Guji , Sun Chengwei, Tan Fuli et al, The compact capacitor bank CQ-1.5 employed in magnetically drivenisentropic compression and high velocity flyer plate experiments, REVIEW OF SCIENTIFIC INSTRUMENTS 79, 053904 ,2008

[14] Lemke R. W., Knudson M. D., Bliss D. E. et al, Magnetically accelerated, ultrahigh velocity flyer plates for shock wave experiments, J. Appl. Phys. 98, 2005:073530-1～9

[15] Wang Guiji, Zhao Jianheng, Tang Xiaosong et al, Study on the technique of electric gun loading for one dimensionally planar strain, Chinese Journal of High Pressure Physics, Vol.19(3), 2005: 269-274

[16] Brechov· Vladimir· Anatonievich, Electrical explosion of conductors and its applications in electrically physical facilities(in Russian), 2000

[17] Chau H.H., Dittbenner G., Hofer W.W. et al, Electric gun: a versatile tool for high-pressure shock wave research, Rev. Sci. Instrum. 51(12), Dec. 1980, P1676～1681

[18] Tucker T.J. , Stanton P.L. , Electrical gurney energy: A new concept in modeling of energy transfer from electrically exploded conductors, SAND-75-0244, May 1975

[19] Schmidt S.C., Seitz W.L., Wackerle Jerry, An empirical model to compute the velocity history of flyers driven by electrically exploding foils, LA-6809, July 1977

[20] He Jia, Simulation on dynamic process of metallic foil electrical explosion driving multi-stage flyers, paper for Master degree, Institute of Fluid Physics, China Academy of Engineering Physics, Mianyang, Sichuan, China, 2007

[21] Asay J.R. and Knudson M.D., Use of pulsed magnetic fields for quasi-isentropic compression experiments, High-Pressure Shock Compression Solids VIII, edited by L.C. Chhabildas, L. Davison and Y. Horie, Springer,2005:329

[22] Davis J. P., Deeney C., Knudson M. D. et al, Magnetically driven isentropic compression to multimegabar pressures using shaped current pulses on the Z accelerator[J]. Physics of Plasma, 12, 2005:056310-1～056310-7

[23] Savage Mark , The Z pulsed power driver since refurbishment,The 13th International Conference on Megagauss Magnetic Field Generation and Related Topics, July 2010.

[24] Zhao Jianheng, Sun Chengwei, Tang Xiaosong et al, The Development of high performance electric gun facility, Experimental Mechanics, Vol.21(3), 2006

[25] Wang Guiji, He Jia, Zhao Jianheng et al, The Techniques of Metallic Foil Electrically Exploding Driving Hypervelocity Flyer to more than 10km/s for Shock Wave Physics Experiments, submitted to Rev. Scie. Instrum., 2011

[26] Wang Guiji, Deng Xiangyang, Tan Fuli et al, Velocity measurement of the small size flyer of an exploding foil initiator, Explosion and Shock Waves, Vol.28(1),2008：28-32

[27] Barker L.M. and Hollenback R.E., Laser interferometer for measuring high velocity of any reflecting surface. J. Appl. Phys., Vol. 43(11),1972: 4669～4675

[28] Weng Jidong , Tan Hua, Wang Xiang et al, Optical-fiber interferometer for velocity measurements with picosecond resolution, Appl. Phys. Lett. 89, 111101,2006

[29] Ao T. , Asay J.R., Chantrenne S. et al., A compact strip-line pulsed power generator for isentropic compression experiments, Rev. Scie. Instrum., 79(1), 013901, 2008

[30] Furnish Michael D., Davis Jean-Paul, Knudson Marcus et al, Using the Saturn Accelerator for Isentropic Compression Experiments (ICE), SAND2001-3773, Sandia National Laboratories, 2001

[31] Hayes D., Backward integration of the equations of motion to correct for free surface perturbaritz, SAND2001-1440, Sandia National Laboratories, 2001

[32] Sun Chengwei, One dimensional shock and detonation wave computation code SSS, Computation Physics, No.3, 1986: 143-145

[33] Burgess T.J., Electrical resistivity model of metals, 1986

[34] Lemke R.W., Knudson M.D. et al., Characterization of magnetically accelerated flyer plates, Phys. Plasmas 10 (4), 1092-1099, 2003

[35] Wang Guiji, Zhao Tonghu, Mo Jianjun et al., Short-duration pulse shock initiation characteristics of a TATB/HMX-based polymer bonded explosive, Explosion and Shock Waves, Vol.27(3), 2007:230-235

[36] Wang Guiji, Zhao Tonghu, Mo Jianjun et al., Run distance to detonation in a TATB/HMX-based explosive, Explosion and Shock Waves, Vol.26(6), 2006:510-515

[37] Sun Chengwei, Dynamic micro-fracture of metals under shock loading by electric gun, J. Phys.IV, Vol.4(8),1994:355-360

[38] Xiong Xin, The spallation of ductile metals under loading of electric gun driven metallic flyer, paper for Master degree, Institute of Fluid Physics, China Academy of Engineering Physics, Mianyang, Sichuan, China, 2007

[39] Hayes D. B., Hall C. A., Asay J. R. et al, Measurement of the Compression Isentrope for 6061-T6 Aluminum to 185 GPa and 46% Volumetric Strain Using Pulsed Magnetic Loading. J. Appl. Phys., Vol.96(10),2004:5520～5527

[40] Wang Ganghua, Experiments, simulation and data processing methods of magnetically driven isentropic compression and highvelocity flyer plates, paper for Ph.D degree, Institute of Fluid Physics, China Academy of Engineering Physics, Mianyang, Sichuan, China, 2008

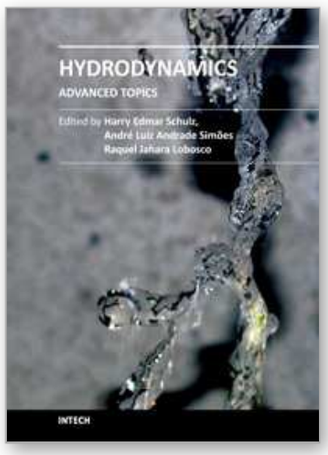

Hydrodynamics - Advanced Topics

Edited by Prof. Harry Schulz

ISBN 978-953-307-596-9

Hard cover, 442 pages

Publisher InTech

Published online 22, December, 2011

Published in print edition December, 2011

The phenomena related to the flow of fluids are generally complex, and difficult to quantify. New approaches - considering points of view still not explored - may introduce useful tools in the study of Hydrodynamics and the related transport phenomena. The details of the flows and the properties of the fluids must be considered on a very small scale perspective. Consequently, new concepts and tools are generated to better describe the fluids and their properties. This volume presents conclusions about advanced topics of calculated and observed flows. It contains eighteen chapters, organized in five sections: 1) Mathematical Models in Fluid Mechanics, 2) Biological Applications and Biohydrodynamics, 3) Detailed Experimental Analyses of Fluids and Flows, 4) Radiation-, Electro-, Magnetohydrodynamics, and Magnetorheology, 5) Special Topics on Simulations and Experimental Data. These chapters present new points of view about methods and tools used in Hydrodynamics.

InTech Europe
University Campus STeP Ri
Slavka Krautzeka 83/A
51000 Rijeka, Croatia
Phone: +385 (51) 770 447
Fax: +385 (51) 686 166
www.intechopen.com

InTech China
Unit 405, Office Block, Hotel Equatorial Shanghai
No.65, Yan An Road (West), Shanghai, 200040, China
中国上海市延安西路65号上海国际贵都大饭店办公楼405单元
Phone: +86-21-62489820
Fax: +86-21-62489821

IntechOpen